

# Black-Box Auditing of Quantum Model: Lifted Differential Privacy with Quantum Canaries

Baobao Song , Shiva Raj Pokhrel , *Senior Member, IEEE*, Athanasios V. Vasilakos , *Senior Member, IEEE*, Tianqing Zhu , *Member, IEEE*, Gang Li , *Senior Member, IEEE*

**Abstract**—Quantum machine learning (QML) promises significant computational advantages, yet models trained on sensitive data risk memorizing individual records, creating serious privacy vulnerabilities. While *quantum differential privacy* (QDP) mechanisms provide theoretical worst-case guarantees, they critically lack empirical verification tools for deployed models. We introduce the first black-box privacy auditing framework for QML based on *Lifted Quantum Differential Privacy*, leveraging quantum canaries—strategically offset-encoded quantum states—to detect memorization and precisely quantify privacy leakage during training. Our framework establishes a rigorous mathematical connection between canary offset and trace distance bounds, deriving empirical lower bounds on privacy budget consumption that bridge the critical gap between theoretical guarantees and practical privacy verification. Comprehensive evaluations across both simulated and physical quantum hardware demonstrate our framework’s effectiveness in measuring actual privacy loss in QML models, enabling robust privacy verification in QML systems.

**Index Terms**—Quantum machine learning, Quantum differential privacy, Privacy auditing

## I. INTRODUCTION

Quantum computing leverages superposition and entanglement to achieve computational advantages over classical systems [1]. Quantum machine learning (QML) exploits these quantum phenomena to potentially accelerate optimization and enable processing of classically intractable problems [2]. However, the enhanced parallel processing capabilities of QML algorithms [3] amplify privacy risks beyond those of classical counterparts. The inherent opacity of quantum systems further complicates privacy analysis and leakage detection [4]. Classical privacy-preserving techniques fail in quantum settings. Differential privacy (DP) requires repeatable data access, but quantum measurement irreversibly collapses quantum states, precluding direct application of classical DP. Additionally, quantum adversaries compromise classical cryptographic protections [5].

Quantum Differential Privacy (QDP) addresses these limitations by ensuring quantum outputs remain  $\epsilon$ -indistinguishable

Received xxx (*Corresponding author: Gang Li*).

Baobao Song is with the Faculty of Engineering and IT, University of Technology Sydney, Sydney, Ultimo, NSW 2007, Australia (email: baobao.song@student.uts.edu.au).

Shiva Raj Pokhrel and Gang Li are with the School of IT, Deakin University, Geelong, VIC 3125, Australia (email: shiva.pokhrel@deakin.edu.au; gang.li@deakin.edu.au).

Athanasios V. Vasilakos is with Center for AI Research (CAIR), University of Agder (UiA), Grimstad, Norway (th.vasilakos@gmail.com).

Tianqing Zhu is with the Faculty of Data Science, City University of Macau, Macau, China (email: Tqzhu@cityu.edu.mo).

for neighboring quantum states differing by small quantum distance [6]. Formally, a quantum mechanism  $\mathcal{M}$  satisfies  $\epsilon$ -QDP if for neighboring states  $\rho, \sigma$  with  $\|\rho - \sigma\|_1 \leq d$ :

$$\mathcal{D}(\mathcal{M}(\rho) \parallel \mathcal{M}(\sigma)) \leq \epsilon \quad (1)$$

where  $\mathcal{D}$  denotes quantum max-relative entropy and  $\epsilon$  is the privacy loss parameter. QDP exploits intrinsic quantum noise (decoherence, measurement uncertainty) as a native privacy resource, eliminating external noise injection [7]. Existing QDP research focuses on mechanism design [6, 7, 8], while privacy auditing for deployed QML models remains unaddressed. The sole auditing technique [4] requires white-box access and provides loose worst-case bounds on  $\epsilon$ , limiting practical applicability.

### A. Motivation

Current QML privacy auditing lacks black-box techniques suitable for realistic deployments. We require an auditing framework satisfying:

- *Black-box operation*: No access to internal circuits, gradients, or training data
- *Statistical estimation*: Quantitative privacy loss bounds rather than binary classification
- *Computational efficiency*: Minimal overhead for regulatory compliance

We propose the first black-box auditing framework for QML models based on Lifted QDP [9]. Our approach introduces **quantum canaries**—offset-encoded quantum states  $|\psi_{\text{offset}}\rangle = e^{-i\frac{\theta}{2}\sigma_a}|\psi\rangle$  designed to detect memorization through controlled perturbations with magnitude  $\theta$ , where  $\sigma_a \in \{X, Y, Z\}$  denotes the Pauli matrix along axis  $a \in \{x, y, z\}$ . The trace distance between original and offset states satisfies:

$$\|\rho - \rho_{\text{offset}}\|_1 = 2|\sin(\theta/2)| \quad (2)$$

for pure states. By analyzing the responses of the model to quantum canaries, we estimate the lower bounds on the effective privacy budget, providing interpretable privacy leakage measures under black-box constraints.

### B. Contributions

Our key contributions are as follows.

- First black-box auditing framework for QML models providing statistically grounded lower bounds on privacy budget via Lifted QDP;

- Introduction of quantum canaries with theoretical guarantees relating offset magnitude  $\theta$  to trace distance; and
- Experimental validation across datasets and quantum circuits, including simulations and real quantum hardware evaluation

Our paper is organized as follows. Section II introduces the necessary background and reviews related work. Section III presents the proposed Lifted QDP for Auditing QML framework, including the construction of quantum canaries and the design of the auditing algorithm. Section IV demonstrates the effectiveness and efficiency of the framework across different datasets and analyzes the impact of various parameter settings. Finally, conclusions and future directions are provided in Section V.

## II. PRELIMINARIES AND RELATED WORK

This section provides the background of QML, QDP, and privacy auditing. First, it introduces the foundational components of quantum algorithms, data encoding methods used to map classical data into quantum states, and representative quantum machine learning (QML) model structures. Section II-A presents the concept of QDP and Lifted QDP, and their typical mechanisms for realization. Section II-B reviews prior work on model auditing and privacy analysis, especially for quantum setting.

Quantum algorithm involves three fundamental stages: initializing an *input quantum state*, evolving the state through unitary operations implemented via *quantum circuits*, and performing *quantum measurements* to obtain classical outputs. In the following, we outline each of stage in turn.

**Input Quantum State** The input to a quantum algorithm is typically qubits, the fundamental units of quantum information. A qubit  $|\psi\rangle$  can exist in a *superposition* of the computational basis states  $|0\rangle$  and  $|1\rangle$ , i.e.,

$$|\psi\rangle = \alpha|0\rangle + \beta|1\rangle, \quad \text{where } |\alpha|^2 + |\beta|^2 = 1. \quad (3)$$

Any pure single-qubit state can be represented as a point on the surface of the *Bloch sphere*, a unit sphere in three-dimensional space. Extending to  $n$  qubits, we take tensor products of the individual Hilbert spaces, therefore forming a  $2^n$ -dimensional Hilbert space.

**Quantum Circuits** A quantum algorithm is typically realized as a quantum circuit, which applies a sequence of quantum gates to an initial state to carry out the desired computation. A quantum gate is a unitary operator  $U$  acting on one or more qubits. These operations can change the states of qubits, including flipping, rotating, creating superposition. Common single-qubit gates include the Pauli gates  $X$ ,  $Y$ , and  $Z$ , the Hadamard gate  $H$ , and the rotation gates  $R_x(\theta)$ ,  $R_y(\theta)$  and  $R_z(\theta)$ , which perform rotations about the respective axes of the Bloch sphere. Multi-qubit gates such as the CNOT gate and controlled- $Z$  gate, operate on two or more qubits and are indispensable for generating entanglement. A quantum circuit of depth  $d$  is an ordered sequence of such gates,

$$\mathcal{E} = U_d \cdots U_2 U_1. \quad (4)$$

A quantum circuit transforms an initial input state into a final quantum state through  $n$  gates. In quantum machine learning,

parameterized quantum circuits are commonly used, where certain gates include tunable parameters optimized during training.

**Quantum Measurement** Quantum measurement is the final step in a quantum algorithm, converting a quantum state into classical information through probabilistic projection onto a measurement basis. This process is modelled by a positive-operator-valued measure (POVM) [10], represented by a set of measurement operators  $\{M_i\}_{i \in \mathcal{O}}$  acting on the Hilbert space, and satisfying the completeness relation  $\sum_i M_i = I$ . Due to finite sampling (i.e., a limited number of repeated circuit executions), the observed outcomes are subject to shot noise, a source of statistical uncertainty.

1) *QML Data Encoding*: Quantum data encoding, also known as quantum feature mapping, refers to the process of embedding classical data into quantum states that can be processed by quantum circuits. Different encoding strategies induces a specific geometry in Hilbert space and affecting the expressive power of the resulting quantum model.

A common encoding method is *angle encoding*, where each feature is mapped to a rotation gate. These gates typically perform rotations around the  $x$ -,  $y$ -, or  $z$ -axis of the Bloch sphere, using gates such as  $R_x(x_i)$ ,  $R_y(x_i)$ , or  $R_z(x_i)$ . For an input vector  $x = (x_1, x_2, \dots, x_d)$ , angle encoding  $R_y$  applies one rotation per feature to an initially prepared  $|0\rangle^{\otimes d}$  state:

$$|\vec{x}\rangle = \bigotimes_{i=1}^n R_y(x_i)|0\rangle. \quad (5)$$

This encoding maps each component  $x_i$  to a quantum rotation and produces a feature-dependent state geometry in Hilbert space. One of the key advantages of angle encoding is its hardware efficiency. It yields encoding layer uses only single-qubit rotations and requires only a linear number of qubits relative to the feature size.

2) *QML Model Structures*: Quantum machine learning (QML) models can generally be classified into three categories: quantum versions of classical algorithms (replicate classical models using quantum circuits), quantum-inspired machine learning (draw on quantum principles to improve classical algorithms) and hybrid classical-quantum models (quantum circuits are integrated into classical machine learning, shown in Figure 1) [11]. Here, we focus on the most widely used category, hybrid QML models, due to their flexibility, trainability, and compatibility with nowadays quantum hardware. In the paper, all QML models in below refer specifically to this hybrid classical-quantum architecture.

QML models combine quantum circuit, typically parameterized quantum circuits (PQCs), with classical components such as optimizers. As shown in Figure 1, classical data is first encoded into quantum states, which are then processed through PQCs to perform transformations. The resulting quantum states are measured and read out into classical information, which is passed to a classical classifier to generate predictions. These predictions are compared with ground truth labels in an evaluation step to compute a loss, which is subsequently used by a classical optimization algorithm to update the parameters of the quantum circuit. This iterative process defines a class of models often referred to as *Hybrid Quantum Neural Networks* [12] (QNNs),

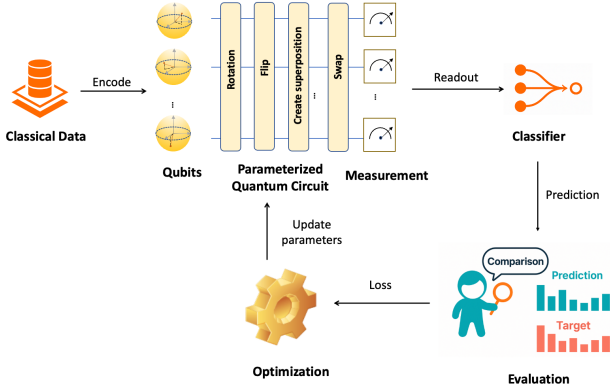


Figure 1: The framework of hybrid classical-quantum models

where the PQC plays a role analogous to a neural network layer in classical deep learning. QNNs leverage both quantum feature encoding and variational transformations, trained via classical feedback, to model complex relationships in data. This hybrid framework is particularly suitable for noisy intermediate-scale quantum (NISQ) devices, as it minimizes quantum resource requirements and leverages the strengths of classical computing.

#### A. QDP and Lifted QDP

*Quantum Differential privacy* (QDP) [6] extends the protective principle of classical Differential Privacy (DP) [13] to quantum-computing settings. It offers a formal guarantee that, for any pair of neighboring quantum input states, the output states produced by a quantum algorithm (e.g. set of instructions that uses quantum bits to process information) are statistically indistinguishable under every possible measurement, ensuring that the addition or removal of a sensitive quantum state does not significantly affect the statistics observable to an adversary. Here, two quantum states are considered neighbors if they are close to each other in terms of a chosen distance metric, such as the trace distance [7], which is the sum of the absolute values of the differences between the eigenvalues of the two states.

**Definition 1: Neighboring Quantum States.** Given two quantum states  $\rho$  and  $\sigma$ , they are considered neighboring if their trace distance is below a certain threshold  $d$ :

$$\tau(\rho, \sigma) = \frac{1}{2} \text{Tr}(|\rho - \sigma|) = \frac{1}{2} \sum_i |\lambda_i(\rho) - \lambda_i(\sigma)| \leq d. \quad (6)$$

where trace  $\text{Tr}(\cdot)$  denotes the matrix trace, and  $\lambda_i(\rho)$  and  $\lambda_i(\sigma)$  denote the eigenvalues of  $\rho$  and  $\sigma$  respectively.

Based on the above definition of neighboring quantum states, the formal definition of QDP is given below.

**Definition 2: Quantum Differential Privacy.** Consider a quantum algorithm  $\mathcal{A} = \{\mathcal{E}, \{M_i\}_{i \in \mathcal{O}}\}$  where  $\mathcal{E}$  is a quantum circuit and  $\{M_i\}_{i \in \mathcal{O}}$  is a set of measurement operators forming a POVM with outcome set  $\mathcal{O}$ . The quantum algorithm  $\mathcal{A}$  satisfies  $(\epsilon, \delta)$ -QDP if for any pair of neighboring quantum states  $\rho$  and  $\sigma$ , and any measurement output  $\mathcal{O}$ , it holds that:

$$\sum_{i \in \mathcal{O}} \text{Tr}[M_i \mathcal{E}(\rho)] \leq e^\epsilon \sum_{i \in \mathcal{O}} \text{Tr}[M_i \mathcal{E}(\sigma)] + \delta \quad (7)$$

where  $\epsilon$  quantifies the privacy loss and  $\delta$  accounts for a small probability of failure in the privacy guarantee. When  $\delta = 0$ , the algorithm satisfies pure  $\epsilon$ -QDP, meaning that the privacy guarantee holds with absolute certainty.

QDP can leverage the intrinsic noise from quantum channels or quantum measurements to achieve privacy protection [9]. Typical channel noises include depolarizing noise [14], which drives a qubit towards the maximally mixed state, and generalised amplitude damping (GAD) noise [15], which causes qubits to lose their excitation and drift toward a thermal equilibrium state. Meanwhile, shot noise in the quantum measurement stage can increase output uncertainty and enhancing privacy. The QDP mechanism for depolarizing noise, GAD noise, and shot noise are described as follows:

**QDP Mechanism of Depolarizing Noise** [6]. Given the trace distance  $d$  of two neighboring qubits and the dimension of the Hilbert space  $D$ , the depolarizing noise channel provides  $\epsilon$ -QDP with

$$\epsilon_{dep} = \ln \left[ 1 + \frac{(1-p)dD}{p} \right] \quad (8)$$

where  $p$  denotes the depolarizing probability.

**QDP Mechanism of Measurement Noise** [16]. Assume the number of measurements is  $N$  and the set of measurement projection operators is  $\{M_i\}$  with maximum rank  $r$  of  $\{M_m\}$ . For quantum states  $\rho$  and  $\sigma$  with  $F(\rho, \sigma) \leq d$ , the measurement process holds  $(\epsilon, \delta)$ -QDP with

$$\epsilon = \frac{Ndr}{\mu(1-\mu)} \left[ \frac{(1-2\mu - Ndr)c^2}{2\mu(1-\mu - Ndr)} + c + \frac{Ndr}{2} \right] \quad (9)$$

where  $\mu = \min\{\mu_1, \mu_0\}$  ( $\mu_0 = \text{Tr}(\rho M_m)$  and  $\mu_1 = \text{Tr}(\sigma M_m)$ ),  $\delta = \sqrt{2\pi}\sigma \text{erfc}\left(\frac{c}{\sqrt{2}\sigma}\right)$ , and  $\sigma = \sqrt{\frac{\mu(1-\mu)}{N}}$ .

As QDP is defined with respect to one fixed pair of neighbouring states, every privacy audit must train a new model on that specific pair and run a separate hypothesis test. Repeating this process for different pairs quickly becomes computationally expensive. Therefore, Lifted QDP [9] is proposed to replace that fixed setup with a randomised neighbouring-state pairs and rejection events drawn from a joint distribution. Randomisation lets many correlated hypothesis tests be re-used on the same trained model, reducing sample complexity and computation, while rejection sets give higher detection power against privacy leaks. The definition of Lifted QDP is:

**Definition 3: Lifted Quantum Differential Privacy.** Let  $P$  represent a joint probability distribution over  $(\rho, \sigma, R)$ , where  $(\rho, \sigma)$  is a pair of random neighboring quantum states and  $R$  is a rejection set. A quantum algorithm  $\mathcal{A} = \{\mathcal{E}, \{M_i\}_{i \in \mathcal{O}}\}$  satisfies  $(\epsilon, \delta)$ -Lifted QDP if, for any quantum measurement  $M$ , the following condition holds:

$$\mathbb{P}_{\mathcal{A}, P} \left[ \sum_{i \in \mathcal{O}} \text{Tr}[M_i \mathcal{E}(\rho)] \in R \right] \leq e^\epsilon \cdot \mathbb{P}_{\mathcal{A}, P} \left[ \sum_{i \in \mathcal{O}} \text{Tr}[M_i \mathcal{E}(\sigma)] \in R \right] + \delta. \quad (10)$$

Lifted QDP turns the single-pair, single-test guarantee of standard QDP into an guarantee over an entire distribution of canaries and tests. Because the auditor can choose a single trained model can be tested many times with different, but statistically correlated, quantum canary pairs  $(\rho, \sigma)$  and rejection sets  $R$ , and the resulting collection of hypothesis

tests can be combined to estimate the privacy leakage. Besides, Lifted QDP can be viewed as a strict generalisation of QDP. When the lifted joint distribution  $\mathcal{P}$  is fixed independently of the algorithm  $\mathcal{A}$ , Lifted QDP is equivalent to QDP [9].

### B. Related Work on Auditing

In classical ML, privacy auditing is a critical technique to empirically assess whether a model conforms to its claimed DP guarantees. A common method is the canary-based audit in black-box setting [17], in which specially crafted examples (called canaries) are injected into the training dataset, and hypothesis testing is performed on the model’s output to determine if those canaries have been memorized. Early audits required training hundreds of models because each hypothesis test compared two separately-trained networks that differed by a single canary [18]. Recent work has significantly reduced this cost by allowing multiple canaries to be tested in parallel within a single training run [19, 20, 21]. Jagielski et al. [21] introduced a deterministic approach by directly injecting multiple canaries into the dataset and conducting multiple hypothesis tests to detect vulnerabilities in DP-SGD. While effective, this method has limitations due to its lack of randomness and diversity, which means it cannot fully address all potential privacy issues. Therefore, Steinke et al. [20] adopted a randomized approach, where canaries are sampled from a Poisson distribution. This method leverages randomness to ensure that canaries are included or excluded independently, which eliminates group privacy concerns, and allows for the reuse of models across multiple tests. Pillutla et al. [19] introduced Lifted DP, which expands the DP definition to handle randomized datasets. By incorporating multiple random canaries, their framework allows for several tests to be run simultaneously using one model. They demonstrated that this framework makes the auditing process significantly more sample-efficient, without compromising the privacy guarantees. Recent advancements in canary-based auditing have also extended to large language models [22, 23], particularly in the context of privacy risks associated with synthetic data generation, where new canary designs have been introduced to enhance the effectiveness of privacy audits, improving both memorization detection and the influence on synthetic data outputs.

However, these classical auditing approaches cannot be directly extended to QML due to fundamental differences between classical and quantum computations. Quantum algorithms operate on quantum states and leverage phenomena such as entanglement and superposition, making their behavior and the impact of privacy mechanisms distinct from classical counterparts. Up to now, Guan et al. [4] is the only one work designed for verifying QDP violations. Unlike classical canary-based black-box auditing, their method employs a white-box approach that directly analyzes the internal quantum operations of algorithms. They systematically examines quantum circuits by analyzing output state distributions through linear algebraic techniques, formulating QDP verification as a mathematical problem involving eigenvalues and eigenvectors of certain matrices derived from quantum operations. The privacy leakage estimated by their method represents an upper bound on  $\epsilon$ , often

approaching theoretical values; however, these estimates are typically excessively high in practical scenarios. Furthermore, the white-box setting of their method limits its applicability in contemporary quantum computing environments, where internal algorithm details may be inaccessible or protected. Consequently, there is a need for a practical auditing method based on statistical hypothesis testing to more estimate actual privacy leakage in QML models.

## III. LIFTED QDP FOR AUDITING QML FRAMEWORK

Based on Lifted QDP, we propose a novel framework to audit QML models effectively. By constructing multiple quantum canaries, this framework enables the tracing of model behavior under subtle, information-carrying perturbations, thereby facilitating the assessment of the model’s privacy protection capabilities. Section III-A formally defines the privacy auditing problem in QML settings, outlining the threat model and auditing objectives. The proposed framework is elaborated in Section III-B, which introduces its core components and the underlying auditing intuition. Section III-C details the construction of quantum canaries via tailored encoding strategies. Section III-D present the Lifted QDP-based Auditing Algorithm for practical deployment.

### A. Problem Statement

Let  $\theta$  denote a QML model trained on a private quantum dataset  $\mathcal{D}$  using a parameterized quantum circuit. The auditor does not have access to the internal structure of  $\theta$ , including its circuit design, Kraus operators, or observables, but is allowed to (i) submit data for training via a training API, and (ii) query the model’s predictions for inputs through an inference interface. The adversary (e.g., the model trainer) is honest-but-unreliable: privacy violations may occur due to misconfigured or insufficiently randomized training procedures, rather than malicious intent. Our goal is to estimate the extent to which the model  $\theta$  has memorized specific training inputs, a phenomenon indicative of privacy leakage( $\epsilon$ ), while minimizing the required sample size. Here, the sample size refers to the number of independent model training runs needed to perform statistical auditing. Therefore, given the  $n$  independent calls to a training oracle  $\text{Train}$ , a trace distance bound  $d$  defining the closeness of neighboring quantum states, and a failure probability  $\beta$ , the auditing model is designed as

$$\mathcal{F}: (\mathbf{Train}, \mathbf{Infer}, d, n, \beta) \mapsto \hat{\epsilon}. \quad (11)$$

### B. Auditing Idea and Framework

Auditing QML models aims to detect whether such models memorize or inadvertently leak information about quantum data. Inspired by classical ML auditing method, we adapt the notion of canaries to the quantum setting by designing *quantum canaries*, quantum-encoded inputs that carry carefully embedded sensitive information. These canaries are constructed to interact with the model in a subtle way, enabling us to probe its internal behavior and infer potential privacy breaches.

The core idea behind auditing QML models is intuitive: if a model memorizes specific training inputs, it is likely to exhibit

distinguishable behavior when exposed to those same inputs again. In our approach, some quantum canaries are inserted into the training data and then reintroduced during testing. By comparing the model’s responses to these trained quantum canaries with those to untrained, unseen quantum canaries, we can infer whether the model has retained information specific to the original quantum canaries. A central challenge of this strategy lies in constructing a rigorous and efficient framework that enables quantifiable detection of such leakage under quantum constraints.

Therefore, we build our auditing framework upon the concept of Lifted QDP. While classical QDP assesses privacy by bounding the distinguishability between the outputs of a quantum mechanism on neighboring quantum states, it inherently considers a fixed auditing setup, typically, a single pair of neighboring states and a specific test condition. This formulation hinders flexibility in the design of auditing mechanisms and leads to high sample complexity, as each privacy test typically requires a fresh model training run and a dedicated hypothesis test. Lifted QDP overcomes these limitations by considering a randomized ensemble of neighboring quantum state pairs and rejection sets drawn from a joint distribution. This expanded formulation enables the use of randomized quantum canaries (from the certain distribution) and supports multiple correlated hypothesis tests per model instance. By leveraging the test statistics induced by quantum canaries, Lifted QDP allows statistical reuse of each trained model, significantly reducing the number of required training runs. Moreover, the use of per quantum canary rejection sets (e.g., a loss-threshold rule learned on separate data) and the adaptive confidence intervals that exploit empirical correlations, boosts auditing power while preserving rigorous finite-sample guarantees. This probabilistic lifting not only retains the core privacy guarantees of standard QDP but also provides a more expressive and sample-efficient foundation for detecting subtle privacy violations in QML models. Building upon this definition, we present a complete auditing framework for QML models, which is shown as Figure 2.

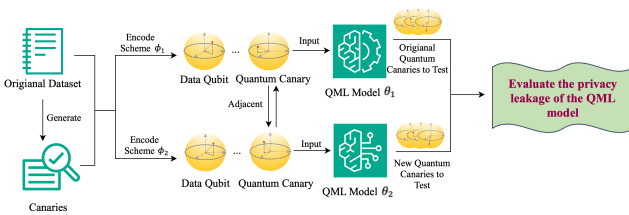


Figure 2: The auditing framework for QML models

In this framework, we begin with an original dataset and generate two equally sized sets of canaries—specially constructed classical data points that are intended to encode sensitive information. These canaries are specially designed to match the statistical characteristics of the original data distribution. One set of canaries is transformed into quantum canaries by applying two quantum encoding schemes  $\phi_1$  and  $\phi_2$ , ensuring that the resulting quantum states satisfy the adjacency condition required by Lifted QDP, namely, a trace distance below a

threshold  $d$ . Both the original dataset and the first set of canaries are independently encoded into quantum states. These states, comprising data qubits and quantum canaries, are then used as input to train two QML models, denoted  $\theta_1$  and  $\theta_2$ . Only the first set of canaries is included in the training phase, while the second set is held out exclusively for evaluation. This setup enables the simulation of randomized ensembles of neighboring quantum states and supports parallel hypothesis testing under Lifted QDP.

During evaluation, both models are tested exclusively on quantum canaries encoded using the same quantum encoding scheme  $\phi_1$  (or  $\phi_2$ ). Importantly, model  $\theta_1$  is tested on the same set of quantum canaries it was trained on, while model  $\theta_2$  is tested on a disjoint set it has never seen during training. We then measure the loss associated with each quantum canary. The loss function is designed to quantify the model’s sensitivity to variations in these inputs, serving as a proxy for how much information the model retains about the first set of encoded quantum canaries. If the loss for QML model  $\theta_1$  (on seen quantum canaries) is significantly lower than the loss for QML model  $\theta_2$  (on unseen quantum canaries), this indicates that  $\theta_1$  has memorized more information about the quantum states, reflecting the presence of quantum memorization and greater privacy leakage. By comparing the losses associated with the quantum canaries across the two models, we can estimate the effective privacy parameter  $\epsilon$  of the QML model, hereby quantifying the degree of leakage and assessing the robustness of the QML model’s privacy protections in a statistically principled and sample-efficient manner.

### C. Construction of Quantum Canaries

Traditional privacy auditing techniques in classical ML rely on canaries—carefully designed data records inserted into the training dataset to probe whether a model memorizes and leaks specific inputs. These canaries are typically raw data samples drawn from or engineered in the input space. Such canaries are inherently classical in nature and in quantum setting (information is represented and manipulated as quantum states), we have to understand privacy leakage in terms of the distinguishability between quantum states. This fundamental shift necessitates the construction of Quantum Canaries, which are quantum-encoded representations of data designed to test the privacy behavior of quantum machine learning models.

Since most QML models encode data one record at a time, we must ensure that every record in the dataset, after encoding, satisfies the definition of adjacency in QDP. To achieve this, we adopt a slightly different encoding method for neighboring records. Specifically, for the original training dataset  $D$ , both models adopt the same angle encoding scheme for all records, namely  $\phi(x) = \pi x$ , where  $x$  denotes the inputs. This ensures consistency in the quantum representations of non-canary data across the two models. The distinction lies in the treatment of the inserted canaries, which is shown in Figure 3. In model  $\theta_1$ , the canaries are encoded identically to the original data using the same angle function  $\phi(c) = \pi c$ , where  $c$  represents the generated canaries. In contrast, model  $\theta_2$  encodes the canaries using a slightly perturbed angle encoding of the form:  $\phi'(c) =$

$\pi * c + \alpha$  where  $\alpha$  is a small offset sampled from a Gaussian distribution  $\mathcal{N}(0, \sigma^2)$ , introduced to induce a bounded change in the resulting quantum state, while maintaining adjacency under QDP.

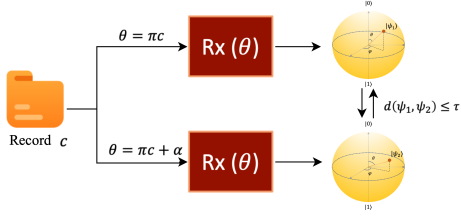


Figure 3: Encode method for constructing quantum canaries

We formally prove the relationship between the offset angle  $\alpha$  and the trace distance upper bound  $d$  in the QDP. The relationship is given as follows:

*Theorem 1:* Consider a classical data vector  $x \in \mathbb{R}^m$  consisting of  $m$  features. Each feature  $c_j$  is encoded into a single qubit using either the  $R_x$  or  $R_y$  rotation gate. We define two encoding schemes  $\phi(c_j) = \pi c_j$  and  $\phi'(c_j) = \pi c_j + \alpha$ , where  $\alpha$  is a offset sampled from a Gaussian distribution  $\mathcal{N}(0, \sigma^2)$ . To ensure that the quantum states produced by the two encodings remain sufficiently close (trace distance less than  $d$ ), the  $\sigma$  is bounded by:

$$\sigma \leq \frac{2 \arcsin(d)}{2.576} \quad (12)$$

PROOF. Given two pure states  $|\psi_1\rangle$  and  $|\psi_2\rangle$ , which are obtained by encoding classical data using the  $R_x$  or  $R_y$  rotation gates, the trace distance is defined as:

$$\tau(|\psi_1\rangle \langle \psi_1|, |\psi_2\rangle \langle \psi_2|) = \sqrt{1 - |\langle \psi_1 | \psi_2 \rangle|^2} \quad (13)$$

Thus, the trace distance for a single qubit is:

$$\tau = \sqrt{\frac{1 - \cos^2(\phi - \phi')}{2}} = \left| \sin\left(\frac{\phi' - \phi}{2}\right) \right| = \left| \sin\left(\frac{\alpha}{2}\right) \right| < d \quad (14)$$

From this we derive the following:

$$|\alpha| < 2 \arcsin(d) \quad (15)$$

Now assume that the offset  $\alpha$  is sampled from a Gaussian distribution, i.e.,  $\alpha \sim \mathcal{N}(0, \sigma^2)$ :

$$P(|\alpha| < 2 \arcsin(d)) = 1 - \delta \quad (16)$$

Therefore,

$$\sigma \leq \frac{2 \arcsin(d)}{\Phi^{-1}(1 - \delta/2)} \quad (17)$$

where  $\Phi^{-1}(\cdot)$  is the inverse cumulative distribution function (inverse CDF) of the standard normal distribution and if we desire  $\delta = 0.01$  (i.e., a 99% probability that the distance is less than  $d$ ), then:

$$\sigma \leq \frac{2 \arcsin(\tau)}{2.576} \quad (18)$$

□

Note that since  $\alpha$  is sampled from a Gaussian distribution, there is always a non-zero probability of sampling values arbitrarily far from the mean. As a result, the inequality in

Theorem 1 holds with high probability (e.g., 99%), but not with absolute certainty. To ensure that the trace distance is strictly bounded by  $d$  for all inputs, a simple remedy is to clip the sampled value of  $\alpha$  to a bounded interval  $[-\gamma, \gamma]$ . With this clipping, we can obtain the following theorem.

*Lemma 1:* Consider a classical data vector  $x \in \mathbb{R}^m$  consisting of  $m$  features. Each feature  $c_j$  is encoded into a single qubit using either the  $R_x$  or  $R_y$  rotation gate. We define two encoding schemes:  $\phi(c_j) = \pi c_j$  and  $\phi'(c_j) = \pi c_j + \alpha$ , where  $\alpha \sim \mathcal{N}(0, \sigma^2)$  is a Gaussian offset. To ensure that the quantum states produced by the two encodings remain within a trace distance less than  $d$ , we apply clipping to the offset as follows:  $\alpha_{\text{clipped}} = \text{Clip}(\alpha, -\gamma, \gamma)$ , and the clipping bound satisfies:

$$\gamma \leq 2 \arcsin(d) \quad (19)$$

To ensure the validity and interpretability of our privacy audit, it is essential that the only difference between the two models lies in the quantum encoding of the canaries. We intentionally avoid applying the encoding scheme  $\phi_2$  to the entire training dataset. This is because encoding all training records in model  $\theta_2$  using the perturbed encoding scheme  $\phi'(x) = (\pi + \alpha)x$  will affect the estimation results and violate the central assumption that the models differ only in the presence and treatment of canaries. In contrast, by restricting the encoding perturbation to the canaries alone, we isolate their contribution to model behavior. This design ensures that any observable difference in model output, particularly on the canary inputs, can be attributed solely to the presence of the quantum canaries themselves. This is critical for evaluating whether a given canary exerts an undue influence on the model and for testing whether such influence leads to a privacy violation under the Lifted QDP.

#### D. Lifted QDP-based Auditing Algorithm

Building upon the auditing framework described in Section III-B and the construction of quantum canaries introduced in Section III-C, we now present the practical auditing algorithm that operationalizes the Lifted QDP-based privacy assessment, which is shown in algorithm 1.

For each of the  $n$  independent trials, we first generate  $2K$  canaries independently from the distribution of original training dataset  $\mathcal{D}$ . The first  $K$  canaries are then appended to the  $\mathcal{D}$  to form an augmented dataset  $\mathcal{D}'$ . Two versions of this augmented dataset are created:  $\mathcal{D}'_0$  and  $\mathcal{D}'_1$ , differing slightly in the applied encoding schemes  $\phi_1$  and  $\phi_2$ , which perturb the angle encoding by an offset parameter. Both datasets are fed into the QML model to initialize two models  $\theta_0$  and  $\theta_1$ , respectively. During evaluation, all  $2K$  canaries are first mapped through the same quantum feature encoding ( $\phi_1$  or  $\phi_2$ ) for fair comparison. The first  $K$  encoded quantum canaries are then input to model  $\theta_0$ , while the remaining  $K$  quantum canaries are input to model  $\theta_1$ . For each input, we compute the corresponding loss value  $l(\theta, c)$ , reflecting the model's prediction error on the respective quantum canary  $c$ , and compare it with a predefined threshold  $\kappa$ . This induces a per quantum canary rejection set  $R(c) = \theta, l(\theta, c) \leq \kappa$ ; the binary decisions  $\mathbb{I}$  is the indicator (memorized or not). We then aggregate  $\mathbb{I}$  across canaries to

---

**Algorithm 1** Lifted QDP for Auditing
 

---

**Input:** Sample size  $n$ , number of canaries  $2K$ , QDP mechanism  $A$ , training set  $\mathcal{D}$ , threshold  $\kappa$ , failure probability  $\beta$ , privacy parameter  $\delta$

**Output:**  $\epsilon$  in QDP

- 1: **for**  $i \in [n]$  **do**
  - 2: Randomly generate  $2K$  canaries  $c_1, c_2, \dots, c_k, \dots, c_{2k}$
  - 3:  $\mathcal{D}' \leftarrow \mathcal{D} \cup \{c_1, \dots, c_k\}$
  - 4: Encode  $\mathcal{D}'$  into qubits using angle encoding scheme  $\phi_1$  and  $\phi_2$  to  $\mathcal{D}_0, \mathcal{D}_1$  respectively
  - 5: Initialize QML with quantum circuit
  - 6: Train two models  $\theta_0 \leftarrow \mathcal{A}(\mathcal{D}'_0)$  and  $\theta_1 \leftarrow \mathcal{A}(\mathcal{D}'_1)$
  - 7: Compute forward pass through QML weights to get prediction and compute loss  $l_{z=1}^K = (f_{\theta_1}(c_z))_{z=1}^K$  and  $l_{j=K+1}^{2K} = (f_{\theta_0}(c_j))_{j=K+1}^{2K}$
  - 8: Record test statistics  $x^{(i)} \leftarrow \mathbb{I}(l_{z=1}^K < \kappa)$  and  $y^{(i)} \leftarrow \mathbb{I}(l_{j=K+1}^{2K} < \kappa)$
  - 9: **end for**
  - 10: Set  $p_1 \leftarrow \text{XBernLower}(\{x^{(i)}\}_{i \in [n]}, \frac{\beta}{2})$  and  $\bar{p}_0 \leftarrow \text{XBernUpper}(\{y^{(i)}\}_{i \in [n]}, \frac{\beta}{2})$
  - 11:  $\hat{\epsilon}_n \leftarrow \log\left(\frac{p_1 - \delta}{\bar{p}_0}\right)$  and a guarantee that  $\mathbb{P}(\epsilon < \hat{\epsilon}_n) \leq \beta$
- 

form the audit statistic, which quantifies potential quantum memorization and privacy leakage.

To achieve statistical validity, each trial records two sets of binary indicators corresponding to whether the canary-injected model and the baseline model satisfy the loss-based detection criterion. Following  $n$  trials, these binary indicators are aggregated and processed through specially designed adaptive confidence interval estimators, namely `XBernLower` and `XBernUpper`, which are based on the `eXchangeable Bernoulli` (`XBern`) distribution [19]. Finally, an empirical privacy loss bound  $\hat{\epsilon}_n$  is computed according to the Lifted QDP condition, ensuring that with high probability at least  $1 - \beta$ , the true privacy loss  $\epsilon$  is bounded by  $\hat{\epsilon}_n$ .

We compare the sample complexity and of our proposed lifted QDP for auditing algorithm (Algorithm 1) with the standard QDP-based auditing algorithm, where each round inserts a single quantum canary and performs one test, which are listed in Table I.

Table I: Sample Complexity Comparison between QDP-based and Lifted QDP-based Auditing

Method	Sample Complexity
QDP	$\mathcal{O}\left(\frac{\ln(1/\beta)}{\Delta^2}\right)$
Lifted QDP	$\mathcal{O}\left(\frac{\ln(1/\beta)}{K\Delta^2}\right)$

Sample complexity refers to the number of independent train-and-test runs required to obtain a reliable lower bound on  $\epsilon$  with confidence  $1 - \beta$ . For QDP based auditing, each run we record a Bernoulli random variable  $Z = 1[\text{loss} < \kappa]$ , where  $\kappa$  is the threshold. Under the hypotheses canary present and canary absent, the success probabilities are  $p_1$  and  $p_0$ . Their gap  $\Delta = |p_1 - p_0|$  is the statistical signal exploited by the audit.

Applying Hoeffding–Chernoff concentration to the empirical mean  $\bar{Z}$  gives the classical bound  $n = \mathcal{O}\left(\frac{\ln(1/\beta)}{\Delta^2}\right)$ . For Lifted QDP, a single run now injects  $K$  canaries simultaneously and declares success only if all  $K$  losses fall below  $\kappa$ . Assuming the  $K$  canaries are approximately independent, in Lifted QDP, sampler complexity is  $\mathcal{O}\left(\frac{\ln(1/\beta)}{K\Delta^2}\right)$  and the theoretical sample complexity is reduced by a factor of  $K$ . There is noted that the saving is an *upper bound* attainable, and in QML experiments, the extra optimization overhead (memory, longer convergence) reduce the effective gap, so the real-world speed-up largely falls short of the ideal one.

## IV. EXPERIMENTS

In this section, we evaluate the effectiveness and efficiency of our proposed *Lifted QDP for Auditing* algorithm by comparing it against standard QDP auditing methods. Specifically, we demonstrate that our method achieves a more accurate bound on the privacy parameter  $\epsilon$ , offering estimates that are closer to theoretical guarantees. Furthermore, we validate its efficiency by reporting a significant reduction in runtime compared to baseline approaches. Section IV-A outlines the datasets and experimental settings used in our evaluation. Section IV-B presents the auditing performance of *Lifted QDP for Auditing*, highlighting both accuracy and computational gains. In Section IV-C, we further investigate how key parameters affect performance. Finally, we summarize key findings and provide insights into the privacy behaviors of QML models in Section IV-D.

### A. Dataset and Setting

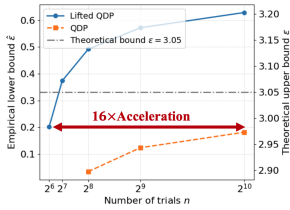
We selected three widely used datasets for our experiments: the Iris dataset [24], Genomic Benchmarks (specifically the Human and Worm subsets) [25], and MNIST [26]. To enable repeated statistical evaluations and reduce computational complexity, we simplified the Genomic Benchmarks and MNIST datasets. For Genomic Benchmarks, we used 200 training samples per class. For MNIST, we selected only digits 0 and 1, using 50 samples from each class for training.

All quantum circuits employed angle encoding for feature mapping and the *RealAmplitudes* ansatz with a linear entanglement strategy. The number of qubits was determined based on dataset complexity: 4 qubits for Iris, 5 for Genomic Benchmarks, and 8 for MNIST. To simulate realistic quantum conditions, we evaluated the models under two types of noise: depolarizing noise and measurement noise. The strength of the depolarizing noise is controlled by a probability parameter  $p$ , which determines the likelihood of a quantum operation being affected by the channel. Measurement noise, on the other hand, is governed by the number of measurement shots  $s$ , where a larger  $s$  reduces the statistical uncertainty and mitigates the impact of sampling errors. We explicitly inserted identity gates into the quantum circuits, one per qubit, to simulate exposure to quantum noise while preserving the circuit logic.

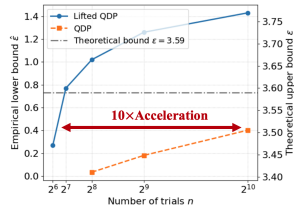
### B. The Auditing Performance

To demonstrate the effectiveness of the proposed Lifted QDP-based auditing algorithm, we compare its empirical estimation

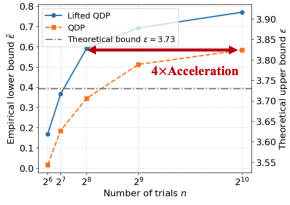
of the privacy parameter  $\hat{\epsilon}$  with that of a baseline QDP-based auditing algorithm under identical trial settings. In addition, to assess the discrepancy between the actual privacy budget and its theoretical guarantee, we introduce another baseline based on the theoretical upper bound of  $\epsilon$ . This theoretical value is proved in [4], which shows that white-box auditing method tends to yield estimates approaching the theoretical maximum privacy loss. As illustrated in Figure 4, each line corresponds to a different experimental configuration. The red curve (QDP) represents the baseline approach, where each trial involves designing and testing a single quantum canary. The blue curve corresponds to the lifted QDP-based auditing method, where each trial incorporates  $K$  quantum canaries simultaneously. The gray line indicates the theoretical upper bound of  $\epsilon$ .



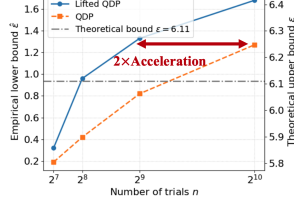
(a) IRIS Dataset with Depolarizing Noise ( $K = 32$ )



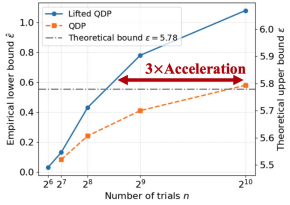
(b) IRIS Dataset with Measurement Noise ( $K = 32$ )



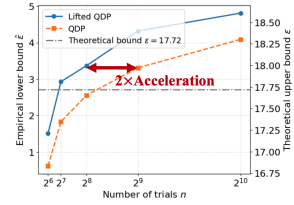
(c) GB Dataset with Depolarizing Noise ( $K = 64$ )



(d) GB Dataset with Measurement Noise ( $K = 64$ )



(e) MNIST Dataset with Depolarizing Noise ( $K = 16$ )



(f) MNIST Dataset with Measurement Noise ( $K = 16$ )

Figure 4: The performance of Lifted QDP auditing under different noise and models

From Figure 4, we first observe a substantial gap between the theoretical and empirical values of  $\epsilon$  in QML models. This discrepancy can be partially attributed to the structural constraints and parameter sparsity inherent in quantum models. For example, certain variational quantum circuits (VQCs) operate within low-dimensional parameter spaces, which limits their expressive capacity. At the same time, such sparsity may induce a natural “compression” effect on individual information, thereby reducing the model’s sensitivity to injected perturbations. As a result, QML models often exhibit stronger empirical robustness against privacy leakage compared to

the theoretical bound (worst-case assumptions). Notably, the empirical–theoretical gap in  $\epsilon$  is larger on MNIST, possibly due to the dimensionality reduction and subsequent mapping to only eight qubits, which compresses the input and reduces the sensitivity.

In addition, when comparing the Lifted QDP-based auditing method with the standard QDP approach, we observe that the number of trials required to reach the same estimated privacy value  $\hat{\epsilon}$  can be reduced by up to 16 $\times$  and at minimum by 2 $\times$ , highlighting the substantial efficiency gains enabled by the lifted design. The actual degree of acceleration depends on both the data distribution and the expressive capacity of the underlying quantum circuit. Moreover, as the number of trials  $n$  increases, the estimated  $\hat{\epsilon}$  also grows and the rate of increase gradually diminishes. This is because, in the early stages, additional trials substantially enhance the identification of model behavior and improve the chance of capturing hidden leakage. However, as  $n$  becomes large, the marginal impact of each new trial diminishes, leading the estimate  $\hat{\epsilon}$  to converge. Finally, we compare the effects of depolarizing noise and measurement noise under the auditing framework across three datasets. We find that for a fixed  $\hat{\epsilon}$ , depolarizing noise achieves acceleration with fewer trials than measurement noise in the majority of settings. This is likely because depolarizing noise acts uniformly on the quantum state, which can amplify subtle differences between neighboring quantum encodings, thereby improving the detectability of privacy leakage signals during auditing.

To further demonstrate the efficiency of the lifted QDP auditing algorithm, we recorded the runtime of models under varying numbers of test canaries, as shown in Table II. Each model is with the number of test canaries  $K$  matching the configurations used in Figure 4. It can be observed that, across different values of  $n$ , the runtime of the QDP increases substantially compared to the Lifted QDP. For the Iris dataset ( $K = 32$ ), the Lifted QDP achieves a runtime speedup of approximately 26 $\times$  over the standard QDP. For MNIST ( $K = 16$ ), we observe about a 10 $\times$  speedup. For the Genomic Benchmarks ( $K = 64$ ), the speedup is even more pronounced: around 30 $\times$  under depolarizing noise and up to 50 $\times$  under measurement noise. The difference in speedup across noise types is mainly driven by times of measurement and quantum circuit complexity. When circuits are relatively simple (fast to train) but involve many measured qubits and a large number of shots, measurement noise tends to deliver more pronounced speedups. Besides, while the theoretical maximum speedup is expected to scale with  $K$ , the observed runtime improvements are slightly smaller. This is because increasing  $K$  also expands the augmented training dataset, which in turn increases the per-model training time. As a result, the actual speedup factor is less than the idealized  $K$ -fold improvement.

**Validation on Real Quantum Hardware:** in order to further validate the practicality of our algorithm, we also used the IRIS dataset and executed the IRIS auditing workflow on a real quantum device via the IBM Quantum platform. Specifically, we deployed our implementation on the `ibm_brisbane` backend. This backend offers mid-scale quantum computation capabilities with support for dynamic circuits and high-fidelity

Table II: Runtime comparison (in minutes) between QDP and Lifted QDP

Dataset-Noise	Method	$2^8$	$2^9$	$2^{10}$	$2^{11}$
IRIS-Depolarizing	QDP	198.90	389.47	780.51	1560.59
	Lifted QDP	7.91	15.42	30.69	60.43
IRIS-Measurement	QDP	106.07	212.88	425.97	851.52
	Lifted QDP	4.18	8.35	16.73	33.39
GB-Depolarizing	QDP	500.62	1099.59	2199.20	4398.92
	Lifted QDP	16.60	32.38	65.88	130.59
GB-Measurement	QDP	399.60	799.11	1598.47	3196.83
	Lifted QDP	7.68	14.99	29.60	58.77
MNIST-Depolarizing	QDP	1889.66	3780.45	7562.43	15127.11
	Lifted QDP	202.02	403.89	808.23	1616.98
MNIST-Measurement	QDP	924.20	1848.53	3698.72	7397.28
	Lifted QDP	68.01	136.73	272.77	544.13

single- and two-qubit gates, making it suitable for executing parameterized quantum circuits under realistic hardware constraints. In addition to standard depolarizing and measurement noise, the `ibm_brisbane` device introduces crosstalk, flux-bias drift, and read-out nonlinearities, sources that are notoriously hard to model faithfully in simulation. By capturing these hardware-specific imperfections, the experiment offers a more realistic assessment of how much memorisation signal survives in practice. Due to runtime limitations imposed by the platform, we only performed a small-scale audit involving  $k = 16$  quantum canaries and 3 independent training runs, each repeated over 3 training epochs. The training and inference process followed our lifted QDP auditing framework, using offset-encoded quantum canaries. The output predictions on the canaries were collected after each training run and statistically aggregated to estimate the empirical privacy leakage.

In this setting, the estimated leakage bound in this setting was  $\hat{\epsilon} = 0.031$ . This small result has two main reasons. First, real quantum hardware introduces additional noise sources beyond depolarizing and measurement noise, which may obscure subtle leakage signals. Second, the small values of  $K$  and  $n$  used in the test limit the statistical power of the audit, naturally resulting in a lower estimate of  $\hat{\epsilon}$ . Moreover, the use of only 3 training epochs may not sufficiently amplify memorization behaviors in the model. Nonetheless, this experiment demonstrates the deployability of our lifted QDP auditing algorithm in practical quantum computing environments.

### C. Parameter Sensitivity Analysis

Beyond the number of trials  $n$ , three additional parameters play a critical role in shaping the auditing performance of the Lifted QDP: the number of quantum canaries per trial  $k$ , the input encoding offset  $\sigma$ , and the noise magnitude (the depolarizing probability  $p$  in depolarizing noise, and the number of measurement shots  $N$  in measurement noise). These parameter effects are illustrated in Figure 5, Figure 8, and Figure 7, respectively.

**The number of quantum canaries  $K$ :** Figure 5 illustrates the estimated values of  $\hat{\epsilon}$  across the three models under both depolarizing and measurement noise, with varying numbers

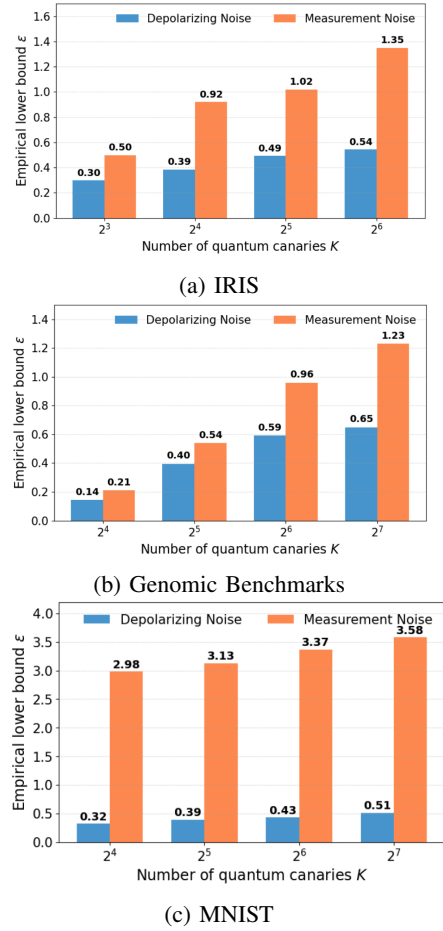


Figure 5: The bound of  $\hat{\epsilon}$  by varying  $K$

of quantum canaries per trial  $K$ . The depolarizing probability was fixed at  $p = 0.01$ , the number of measurement shots was set to  $N = 32$ , and the number of trials was set to  $n = 256$ . We observe that as  $k$  increases, the estimated  $\hat{\epsilon}$  also increases, but the rate of growth gradually diminishes. This trend can be attributed to the fact that when  $K$  is small, adding each additional quantum canary significantly amplifies the probability difference, thereby increasing the measured privacy budget. However, as  $k$  continues to grow, the event space begins to saturate success probabilities approach 0 or 1, leading to diminishing marginal contributions from each added quantum canary.

In addition, we observe that in Figure 5a, when the theoretical privacy bounds for both noise types are close,  $\hat{\epsilon}$  under measurement noise are consistently higher than those under depolarizing noise. This suggests that, for a given privacy budget, applying depolarizing noise results in lower actual privacy leakage compared to measurement noise. One possible explanation is that depolarizing noise introduces uniform perturbations in quantum channel, which may obscure fine-grained model behavior more effectively. In contrast, measurement noise affects only the readout layer and may leave deeper model-level memorization signals intact, thus leading to greater effective leakage. These findings highlight the importance of noise model selection in QML privacy protection: even

when theoretical bounds are comparable, the practical leakage behavior can vary considerably, and depolarizing noise may offer stronger empirical privacy guarantees under the same theoretical constraints.

**The encoding offset  $\sigma$ :** We further investigate how the input encoding offset  $\sigma$  affect the estimated lower bound of  $\hat{\epsilon}$ . To begin with, we visualize how different values of  $\sigma$  influence the angle distribution of individual qubit after encoding, as shown in Figure 6. Here, the encoding scheme  $\phi_1$  refers to direct mapping, while  $\phi_2$  applies an additive angular offset sampled from a Gaussian distribution with standard deviation  $\sigma$ . As illustrated, when  $\sigma$  is small, the distributions of qubit angles under  $\phi_1$  and  $\phi_2$  remain almost indistinguishable, indicating negligible perturbation at the encoding level. As  $\sigma$  increases, the angular spread under  $\phi_2$  becomes significantly broader, resulting in larger trace distances between the quantum states produced by the two encoding schemes. This growing separation directly impacts the level of privacy leakage observed: since greater trace distance corresponds to larger distinguishability between neighboring quantum states, the privacy budget also increases accordingly.

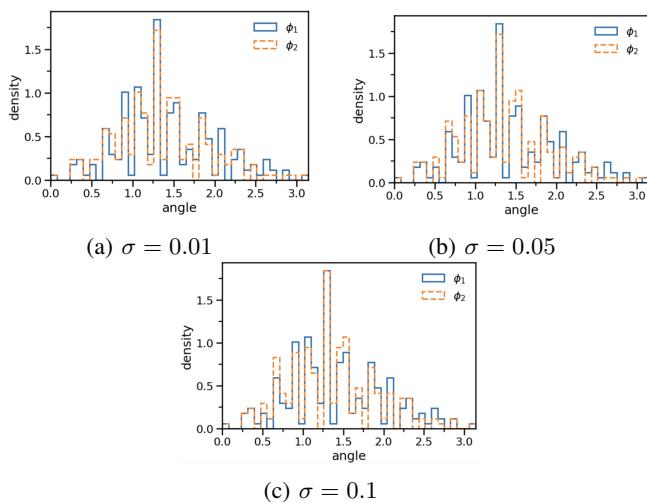


Figure 6: Distribution of qubit angles after different encoding schemes

In Figure 7, increasing the value of  $\sigma$  always pushes the empirical estimate  $\hat{\epsilon}$  upward across different noise settings. According to Lemma 1,  $\sigma$  directly influences the bound on the trace distance between encoded quantum states, which in turn affects the privacy budget bound. Moreover, the increase effect becomes more evident when the shot number  $n$  is large. When  $n$  is small, the count statistics are coarse, so  $\hat{\epsilon}$  is systematically under-estimated and different  $\sigma$  values are partially “masked” by the large sampling variance. As  $n$  grows, the estimator approaches its asymptotic (unbiased) regime, and the contribution of  $\sigma$  emerges clearly, causing the gaps between curves to widen.

**Noise magnitude ( $p$  or  $N$ ):** Figure 8 illustrates the relationship between noise amplitude and the estimated privacy budget  $\hat{\epsilon}$ . As indicated by (8) and (9), decreasing the depolarizing probability  $p$  or increasing the number of measurement shots

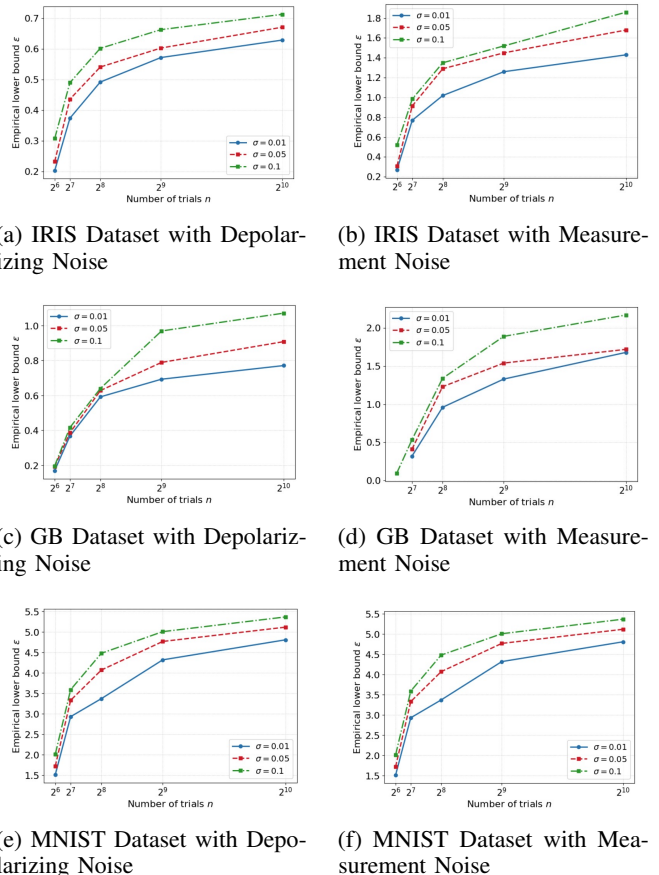


Figure 7: The relationship between  $\hat{\epsilon}$  and  $\sigma$

$N$  leads to a reduction in  $\hat{\epsilon}$ . This is intuitive: a smaller  $p$  means a lower chance of qubit depolarization, while a larger  $N$  reduces statistical uncertainty in measurements, both resulting in less noise and improved privacy protection. In addition, we observe that when the number of trials  $n$  is small, varying  $p$  or  $N$  has little impact on the estimated  $\hat{\epsilon}$ . This is because under limited sampling, the dominant source of error arises from statistical variance rather than noise amplitude. Only when  $n$  is sufficiently large do the benefits of reducing depolarization or increasing measurement precision manifest more clearly in the observed privacy budget estimates.

#### D. Finding and Discussion

Our simulations and hardware runs show that QML models offer a built-in privacy advantage over classical models. In practice, QML models leak less information than their theoretical privacy budgets predict. Three factors explain this: (i) limited circuit expressivity keeps variational quantum circuits from fitting arbitrarily complex decision boundaries; (ii) barren plateaus hamper optimization [27], preventing the model from memorizing the training set; and (iii) hardware noise injects randomness that further obscures individual records. Moreover, real-world QML models usually compress high-dimensional data before encoding it into the small number of qubits, discarding fine-grained details and lowering leakage risk even more. These properties make QML especially attractive for

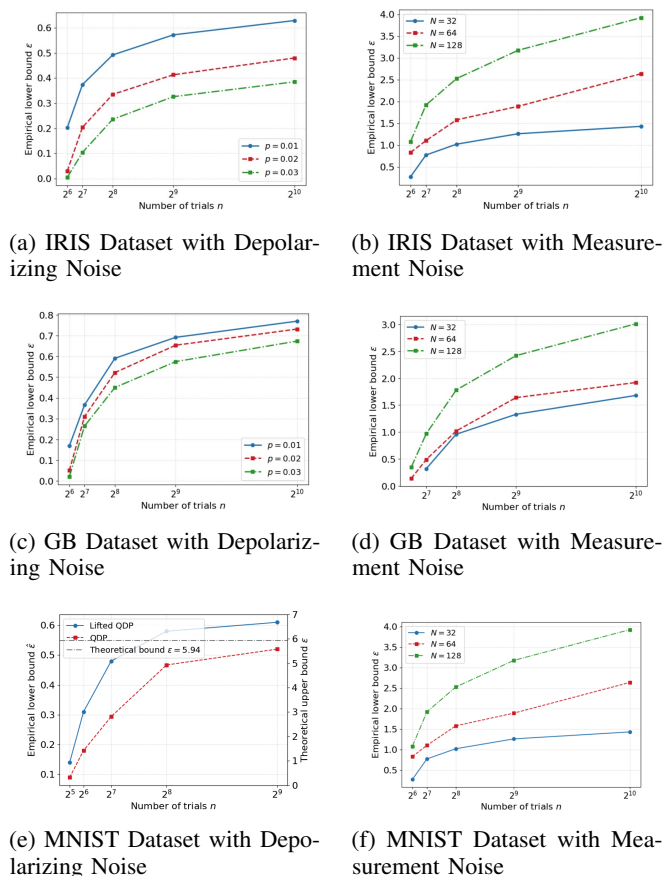


Figure 8: The relationship between the  $\hat{\epsilon}$  and noise amplitude

privacy-critical domains, such as healthcare or genomics, where a slight trade-off in accuracy is acceptable in exchange for stronger protection of sensitive data.

We also observe that, for a fixed theoretical privacy budget, depolarizing noise tends to yield stronger empirical privacy guarantees than measurement noise. This finding implies that, when apportioning the overall privacy budget, we can allocate a smaller share to the depolarizing channel and reserve a larger share for the measurement stage, thereby further reducing the risk of privacy leakage in practice.

Within the Lifted QDP auditing framework, introducing multiple quantum canaries can drastically shorten the time needed to estimate privacy leakage and produces  $\hat{\epsilon}$  values that more closely match the theoretical bound. It is important to emphasize,  $\hat{\epsilon}$  depends on far more than the listed parameters, canary count  $K$ , trial number  $n$ , and offset  $\sigma$ . Additional factors such as circuit depth and the distribution of data also influence the effective leakage; many of these details are hidden in a black-box setting, which is precisely why black-box auditing is necessary. The present experiments therefore serve only to demonstrate the feasibility and efficiency of the Lifted QDP auditing framework. They should not be interpreted as a universal rule that adding a given amount of theoretical noise will always produce a proportional reduction in leakage; each model-hardware combination must be assessed on its own terms.

## V. CONCLUSION

We present a novel black-box auditing framework for evaluating privacy leakage in QML models. Unlike prior white-box approaches providing only theoretical upper bounds, our method leverages *Lifted QDP* to estimate empirical privacy leakage using black-box access only. At the core of our framework are quantum canaries—offset-encoded quantum states inserted into training data to probe model memorization. By analyzing model responses to these canaries at inference, we estimate lower bounds on the privacy budget  $\epsilon$ , providing interpretable, data-driven privacy assessment. This bridges theoretical privacy guarantees with practical auditing in deployment settings where model internals are inaccessible. We validate the framework through extensive simulations and real quantum hardware evaluations, demonstrating effectiveness for real-world QML privacy auditing.

Our framework has three key limitations. First, quantum canaries use Gaussian-sampled fixed offsets independent of model dynamics, potentially failing to detect localized memorization or adversarial obfuscation. Second, experiments isolate single noise sources, while real quantum hardware exhibits simultaneous, interacting noise channels that may alter privacy estimates. Finally, we address only differential privacy leakage, omitting broader inference threats (membership, attribute, property inference).

*Future Work.* Future directions include: i) adaptive quantum canary generation aligned with model representations, ii) joint modeling of multiple noise sources under Lifted QDP, and iii) extension to comprehensive inference threat evaluation for holistic adversarial robustness assessment.

## REFERENCES

- [1] M. A. Nielsen and I. L. Chuang, *Quantum computation and quantum information*. Cambridge university press Cambridge, 2001, vol. 2.
- [2] S. Khurana, M. Nene, and M. Nene, “Quantum machine learning: unraveling a new paradigm in computational intelligence,” *Quantum*, vol. 74, no. 1, 2024.
- [3] J. Lopez, “Quantum machine learning: Applications, algorithms, and hardware challenges,” *International Journal of AI, BigData, Computational and Management Studies*, vol. 5, no. 4, pp. 1–13, 2024.
- [4] J. Guan, W. Fang, M. Huang, and M. Ying, “Detecting violations of differential privacy for quantum algorithms,” in *Proceedings of the 2023 ACM SIGSAC Conference on Computer and Communications Security*, 2023, pp. 2277–2291.
- [5] J. J. Tom, N. P. Anebo, B. A. Onyekwelu, A. Wilfred, and R. Eyo, “Quantum computers and algorithms: a threat to classical cryptographic systems,” *Int. J. Eng. Adv. Technol.*, vol. 12, no. 5, pp. 25–38, 2023.
- [6] L. Zhou and M. Ying, “Differential privacy in quantum computation,” in *2017 IEEE 30th Computer Security Foundations Symposium (CSF)*. IEEE, 2017, pp. 249–262.
- [7] C. Hirche, C. Rouz e, and D. S. Fran a, “Quantum differential privacy: An information theory perspective,” *IEEE Transactions on Information Theory*, 2023.

- [8] Y.-R. Bai, Y.-H. Tao, S.-H. Wu, H. Zhang, and S.-M. Fei, "Quantum differential privacy under noise channels," *Physica Scripta*, vol. 99, no. 3, p. 035119, 2024.
- [9] B. Song, S. R. Pokhrel, A. V. Vasilakos, T. Zhu, and G. Li, "Towards a hybrid quantum differential privacy," *IEEE Journal on Selected Areas in Communications*, pp. 1–1, 2025.
- [10] M. Oszmaniec, L. Guerini, P. Wittek, and A. Acín, "Simulating positive-operator-valued measures wif projective measurements," *Physical review letters*, vol. 119, no. 19, p. 190501, 2017.
- [11] A. Zeguendry, Z. Jarir, and M. Quafafou, "Quantum machine learning: A review and case studies," *Entropy*, vol. 25, no. 2, p. 287, 2023.
- [12] S. Adhikary, S. Dangwal, and D. Bhowmik, "Supervised learning with a quantum classifier using multi-level systems," *Quantum Information Processing*, vol. 19, pp. 1–12, 2020.
- [13] C. Dwork, "Differential privacy," in *International Colloquium on Automata, Languages, and Programming*. Springer, 2006, pp. 1–12.
- [14] Y. Du, M.-H. Hsieh, T. Liu, D. Tao, and N. Liu, "Quantum noise protects quantum classifiers against adversaries," *Physical Review Research*, vol. 3, no. 2, p. 023153, 2021.
- [15] R. Srikanth and S. Banerjee, "Squeezed generalized amplitude damping channel," *Physical Review A*, vol. 77, no. 1, p. 012318, 2008.
- [16] Y. Li, Y. Zhao, X. Zhang, H. Zhong, M. Pan, and C. Zhang, "Differential privacy preserving quantum computing via projection operator measurements," *arXiv preprint arXiv:2312.08210*, 2023.
- [17] I. Namatevs, K. Sudars, A. Nikulins, and K. Ozols, "Privacy auditing in differential private machine learning: The current trends." *Applied Sciences (2076-3417)*, vol. 15, no. 2, 2025.
- [18] N. Carlini, C. Liu, Ú. Erlingsson, J. Kos, and D. Song, "The secret sharer: Evaluating and testing unintended memorization in neural networks," in *28th USENIX security symposium (USENIX security 19)*, 2019, pp. 267–284.
- [19] K. Pillutla, G. Andrew, P. Kairouz, H. B. McMahan, A. Oprea, and S. Oh, "Unleashing the power of randomization in auditing differentially private ml," *Advances in Neural Information Processing Systems*, vol. 36, 2024.
- [20] T. Steinke, M. Nasr, and M. Jagielski, "Privacy auditing with one (1) training run," *Advances in Neural Information Processing Systems*, vol. 36, pp. 49 268–49 280, 2023.
- [21] M. Jagielski, J. Ullman, and A. Oprea, "Auditing differentially private machine learning: How private is private sgd?" *Advances in Neural Information Processing Systems*, vol. 33, pp. 22 205–22 216, 2020.
- [22] A. Panda, X. Tang, M. Nasr, C. A. Choquette-Choo, and P. Mittal, "Privacy auditing of large language models," *arXiv preprint arXiv:2503.06808*, 2025.
- [23] M. Meeus, L. Wutschitz, S. Zanella-Béguelin, S. Tople, and R. Shokri, "The canary's echo: Auditing privacy risks of llm-generated synthetic text," *arXiv preprint arXiv:2502.14921*, 2025.
- [24] S. Tomal, A. A. Shafin, A. Afaf, and D. Bhattacharjee, "Quantum convolutional neural network: A hybrid quantum-classical approach for iris dataset classification," *arXiv preprint arXiv:2410.16344*, 2024.
- [25] N. Singh and S. R. Pokhrel, "Modeling quantum machine learning for genomic data analysis," *arXiv preprint arXiv:2501.08193*, 2025.
- [26] A. Senokosov, A. Sedykh, A. Sagingalieva, B. Kyriacou, and A. Melnikov, "Quantum machine learning for image classification," *Machine Learning: Science and Technology*, vol. 5, no. 1, p. 015040, 2024.
- [27] J. R. McClean, S. Boixo, V. N. Smelyanskiy, R. Babbush, and H. Neven, "Barren plateaus in quantum neural network training landscapes," *Nature Communications*, vol. 9, no. 1, p. 4812, 2018.